Computational investigation of dimethoate and β-Cyclodextrin inclusion complex: molecular structures, intermolecular interactions and electronic analysis

Amina Benaissa (a.benaissa@univ-skikda.dz)
University 20 Aout 1955 Skikda
Abdelaziz Bouhadiba
University 20 Aout 1955 Skikda
Noura Naili
University 20 Aout 1955 Skikda
Faiza Chekkal
University 20 Aout 1955 Skikda
Malika Khelfaoui
University 20 Aout 1955 Skikda
Bouras Ibtissem
University 20 Aout 1955 Skikda
Mehri Karima
University 20 Aout 1955 Skikda
Mohamed Salah Madjram
University 20 Aout 1955 Skikda
Bachir Zouchoune
University Ben M'hidi Oum el Bouaghi
Sulaiman Mogalli
University 20 Aout 1955 Skikda
Najran Malfi
University 20 Aout 1955 Skikda
Leila Nouar
University of 08 Mai 1945 Guelma, Algeria
Fatiha Madi
University of 08 Mai 1945 Guelma, Algeria

Research Article

Keywords: β-cyclodextrin dimethoate inclusion complexes, DFT, NBO, QTAIM, NCI, IGM

Posted Date: December 29th, 2022

DOI: https://doi.org/10.21203/rs.3.rs-2372447/v1

Additional Declarations: No competing interests reported.

Version of Record: A version of this preprint was published at Structural Chemistry on March 29th, 2023. See the published version at https://doi.org/10.1007/s11224-023-02162-8.

Abstract

The proposed study concerns the inclusion complexation of dimethoate (DMT) in the β-cyclodextrin (β-CD) molecule cage using a 1:1 stoichiometry. The interactions between DMT and -CD were evaluated using PM7 and DFT in water and gas with base 6-31G(d,p); using the CAMB3LYP functional. All approaches agree with the optimal 3D structure, which includes full DMT inclusion in the CD cavity. Complexation, LUMO, and HOMO energies were computed. The natural bond orbital (NBO) and UV- visible calculations were determined and discussed. Additionally, the non-covalent intermolecular interactions between dimethoate and β-cyclodextrin are investigated through: reduced density gradient (RDG), non-covalent interaction (NCI) and independent gradient model (IGM) that the main forces stabilizing the examined inclusion complex are H-bond and Van Der Waals interactions. Furthermore, the energy decomposition analysis (EDA) emphasizes the importance of the H-bond as attractive interactions.

Introduction

Recently, the scientific community certified that phytosanitary agents and their metabolites are harmful against the environment. The use of pesticides in agriculture presents an ecotoxicological risk [1, 2]. They found that pesticides regularly exceed ecological quality thresholds [3–5] and constitute a significant factor in shaping aquatic species and sediment. Besides; they threaten human health using water, fish consumption, and marine species [6–10].

Organophosphate pesticides are the most widely used insecticides on the planet causing quick environmental degradation. The ecological difficulties are created by high doses of pesticides and the number of applications in agriculture [11].

Indeed, Dimethoate is an organophosphate pesticide used to combat the losses due to pests like fungi and insects [12].

Inorganic insecticide dimethoate (Fig. 1. **a**) presents the potential to harm the nervous system. Both an insecticide and an acaricide serve their purpose well. Insects' and human's neurological systems depend on cholinesterase consisting of an enzyme these chemicals aim to prevent from doing their job.

Pesticide pollution of the aquatic ecosystem can result in acute and chronic intoxication of fish and other species. These findings show that fish were harmed by dimethoate poisoning [13–15].

Therefore, dimethoate is complexed with supramolecular structures involving inclusion complexes with cyclodextrins to remediate the pesticide pollution problem. Cyclodextrins are commonly used for water treatment. They retain a lot of pesticides, insecticides, metals or toxic organic compounds such as phenols; thus, purifying running water [17, 18].

Cyclodextrin is a molecule cage of natural origin that creates an opportunity to encapsulate different compounds. Microcapsule technology's carrier matrix, cyclodextrin, and its derivatives are widely employed in many culinary and medicinal goods, prompting much scientific investigation [17].

Cyclodextrin (CD) is a cyclic oligomer consisting of α-D glucopyranose units. The most typical forms of CDs are 6, 7, and 8 α -1,4-D-glucopyranose, often known as α-, β-, and γ- CD, respectively [19].

Due to their particular molecular structure, which consists of an exterior hydrophilic and an interior cavity that is hydrophobic, they can form inclusion complexes with a variety of guest molecules that have the appropriate polarity and dimensions [20–22].

As known, theβ-CD (Fig. 1. **b**) is the most commonly used for the formation of inclusion complexes with a variety of products through the interactions of van der Waals types (vdW) [23]. Cyclodextrin has an internal cage as well as a truncated cone with a diameter of 6-6.4Å and a depth of 8 Å. It is important to develop inclusion complexes of organic compounds with cyclodextrins for technological and medicinal aims [24–30].

In this regard, Goran M. Petrovi et al. investigated by UV spectrophotometry the interaction and solubility of dimethoate with an aqueous solution of β-cyclodextrin (mβCD) [31]. It is possible to effectively use mβ-CD in pesticide solution formulations to boost the bioavailability and biodegradability of the researched pesticides based on the solubility augmentation observed in the investigated pesticides in the aqueous solution of mβ-CD.

Furthermore, the authors omitted to clarify the mechanism of inclusion with β-CD despite the variety of characterization used approaches gain depth in sight into the inclusion of complex formation between dimethoate and β-CD. Until now, there is no theoretical investigation using DFT calculations to evaluate the interactions between dimethoate and β-cyclodextrin.

Thus, this study is provided in gas and aqueous phases to describe the nature of non-covalent inter-molecular interactions, namely the H-bond ones between DMT and β-CD during the inclusion of complex formation.

In order to identify the nature of the interaction between host and guest, we applied natural bond orbitals (NBO), energy decomposition analysis (EDA), quantum theory of atoms in molecules (QTAIM), non-covalent interactions-reduced density gradient (NCI-RDG) and Independent gradient model (IGM).

Computational Methods

DFT calculations were carried out with Gaussian 09 software package [32] and the creation of molecular graphs was carried out by the Gauss view 6 programs [33].

The structure of dimethoate was obtained for the first part of our investigation from the PubChem compound database [34]. Additionally, Chem Office 3D Ultra was used to build the structure of the β-CD (version 10, Cambridge software) [35]. After that, each configuration was fully optimized using the MOPAC 2016 package's semi-empirical approach PM7 [36].

The initial inclusion structures of DMT and β-CD were constructed by the HYPER CHEM version 7.5 molecular modeling program [37]. The guest dimethoate was moved to enter and cross the host cavity of β-CD along the Z axis from − 6 to 6 with one pass in each of the two possible directions A and B (see Fig. 2a). The PM7 approach was used to optimize the created structures at each step without any restrictions and the most stable complexes were identified. The created structures at each step were optimized at the PM7 method without any symmetrical restrictions deducing the most stable complexes.

To get more accurate results, we optimized the free guest, free host, and most stable complexes using density functional theory (DFT) [38–41] including dispersion correction [42–44] by means of CAM/B3LYP for estimating non-covalent interactions particular those of hydrogen bonding interactions [45, 46], with 6–31/ G(d, p) basis set in the gas phase and water aqueous phase.

The solvent effect on conformational equilibrium was introduced in the single point DFT calculation of water (= 78.5) using the conductor polarizable continuum model (CPCM) [47]. Global reactivity indices were determined using the HOMO-LUMO transitions reactivity indices obtained by means of HOMO-LUMO transitions.

According to the minimum energy structure, the Complexation energy upon complexes between dimethoate and Beta cyclodextrin is given by Eq. (1) [48]:

$$E_{complexation} = E_{complex} - (E_{free\beta-CD} + E_{freeDMT})$$

1

Where $E_{complex}$ $E_{freeDMT}$ and $E_{free\beta\text{-}CD}$ correspond to Heat formation (HF) energies of the complex, the free guest DMT and the free host β -CD, respectively.

The intensity of the energy variation would be a sign of the force driving toward complexes.

The interaction and deformation energy (DEF) for each host and guest component during complex formation is the difference between the optimized component compared to its energy in the complex (Eq. (2)) [49]:

$$E_{\text{Interaction}} = E_{\text{Complex}} - \left(E^{SP}_{\beta-CDincomplex} + E^{SP}_{DMTincomplex}\right)$$

2

where ESPβ-CD and ESPDMT correspond to the single point energy of the β-CD and DMT in the optimized complex respectively.

$$E^{DEF} = E_{(component)spopt} - E_{(component)opt}$$

3

Where $E_{(component)spopt}$ is the single point energy of the component using its geometry in the optimized complex, and $E_{(component)opt}$ is the energy of the optimized geometry of the component.

The difference between the energy of the fully optimized component and its energy in the complex was used to determine the deformation energy for each component, host, and guest during the complex's formation [50].

The charge transfer between the β-CD molecule and the DMT has been taken into account using natural bond orbital NBO population analyses [51–53]. Additionally, absorption spectra of the DMT@β-CD complexes have been calculated by time-dependent-density functional theory (TD/DFT) at CAM B3LYP/ 6-31G(d, p) level [54].

QTAIM, NCI-RDG, and IGM analysis were explored using the Multiwfn program [55] and visualized by the VMD program [56].

Results And Discussion

Energetic and structural analysis of complexes

The PM7 calculation was established for models A and B to control the complexation energy during the inclusion process of DMT in the β-CD cavity from − 7 to + 7 to identify global minimums energy.

Figure 2 shows the variation of the complexation energy (ΔE) during the inclusion process of both models as A and B are a function of the Z distance. These results indicate that the complexation energy values are negative, implying that the DMT@ β -CD produced complexes are energetically favorable [56, 57]. For both A and B orientations, the global minimums of the most stable structures are situated at Z = -2Å.

From Fig. 3, it can be seen that the complexation energy values obtained are − 42.86 kcal/mol and − 44kcal/mol for orientations A and B respectively.

According to PM7 calculations evaluating the complexation energies show that orientation B gives rise to the conformer which is more stable by 1.14 kcal/mol than that corresponding to orientation A.

The calculated complexation and interaction energies in gas and aqueous phases with the functional CAM-B3LYP for Orientations A and B are provided in Table 1.

However, orientation B provides the most significant values of E encapsulation. Aqueous phase interaction energies lend support to gas phase interaction energies. Compared to orientation A, orientation B has stronger negative energy. Additionally, we can see that the interaction energy difference in the gas and aqueous phases, respectively, is 1.48 kcal/mol and 8.708 kcal/mol, supporting the stability of orientation B.

The results also revealed that the $\Delta E_{interaction}$ energy of the β-CD molecule with functional CAM-B3LYP 6-31G (d, p) is higher than that of the DMT molecule in the two orientations A and B. $E_{interaction}$ is a crucial measure in assessing the stability of inclusion complexes.

In addition, $\Delta E_{interaction}$ is an important parameter measuring the stability of inclusion complexes; the results reveal that the deformation energy of the β-CD molecule with functional CAM-B3LYP 6-31G (d, p) is higher than that of the DMT molecule in the two orientations. This interaction energy demonstrates that the -CD structure's flexibility is crucial for increasing intermolecular interaction and the entire system's stability after complexation.

Table1 The complexation energies computed in gas and in aqueous phases with the functional CAM-B3LYP for A and B orientations.

	In gas		In water	
	Orientation A	Orientation B	Orientation A	Orientation B
$E_{encapsulation}$ (kcal/mol)	-16.46	-17.85	-10.726	-10.753
$\Delta E_{interaction}$ (kcal/mol)	-17.12	-30.40	-12.215	-20.923
ΔE_{DEF}(DMT) (kcal/mol)	-0.516	3.78	-0.131	2.581
$\Delta E_{DEF}(\beta - CD)$(kcal/mol)	1,18	8.76	1.594	7.615

Figure 4 shows the favorable structures of the lowest energy conformers obtained in the water and gas phase using the CAM-B3LYP functional. It is clear from the structures that the DMT molecule is completely encapsulated in the β-CD cavity, when the intermolecular hydrogen bonds (HBs) in both structures control the stabilization between the two orientations, A and B, in different phases.

Electronic Properties

TD-DFT analysis

The UV–Vis spectra are obtained using the DTDFT method with CAM-B3LYP functional and 6-31G(d,p) basis set in water, to identify variation electron transitions [58]. The absorption wavelength, the oscillator strength (f), and minor and major orbital contributions, as well as their predicted energies (E), have been reproduced and shown in **Fig. 5**.

The HOMO and LUMO orbitals of the two orientations are entirely localized on the DMT. These results revealed that encapsulation does not change the guest molecule's charge distribution.

Table 2 shows that the absorption spectra of free DMT have three absorption bands located at 226.33, 212.93, and 201.51 nm, corresponding to transition energies of 5.48, 5.82, and 6.15 eV respectively. These peaks mainly originated due to electronic transition from HOMO-3→ LUMO (47.17%), HOMO→ LUMO + 1(57.29%), and HOMO → LUMO 51.83%.

Both orientations' UV-vis absorbance after complexation with β-CD differs from that of free DMT. It has been proposed that these variations in the absorption bands are generated by conformational changes in the structure of DMT that occur when the inclusion complex with β-CD is formed.

Both orientations' UV–vis absorbance changes after complexation with β-CD. Variations in absorption bands may be due to conformational changes in DMT during inclusion complex formation with β -CD.

Table 2 Absorption peak (λ), the predicted energies (E), oscillators strength (f), and contribution of orbital in water for the two orientations A and B

	Band	λ(nm)	E(eV)	f(um)	Minor and major orbital contribution	
DMT	Band 1	226.33	5.48	0.0078	(HOMO-3) → (LUMO)	47.17%
					(HOMO) → (LUMO)	41.79%
					(HOMO-3) → (LUMO+3)	14.27%
					(HOMO-3) → (LUMO+4)	11.37%
	Band 2	212.93	5.82	0.0003	(HOMO) → (LUMO1+)	57.29%
					(HOMO-4) → (LUMO)	25.16%
					(HOMO-4) → (LUMO+1)	18.73%
					(HOMO-3) → (LUMO+4)	10.52%
	Band 3	201.51	6.15	0.0022	(HOMO) → (LUMO)	32.53%
					(HOMO) → (LUMO+1)	30.31%
Orientation A	Band 1	223.12	5.56	0.013	(HOMO) → (LUMO+1)	34.47 %
					(HOMO) → (LUMO)	27.79 %
					(HOMO -1) → (LUMO)	15.12 %
					(HOMO-8) → LUMO+4)	15.10 %
					(HOMO -1) → (LUMO+1)	14.62 %
	Band 2	213.59	5.80	0.0049	(HOMO) → (LUMO)	48.61 %
					(HOMO-26) → LUMO+1)	17.77 %
	Band 3	201.71	6.14	0.0121	(HOMO -1) → (LUMO+1)	42.81%
					(HOMO -2) → (LUMO1)	28.23 %
Orientation B	Band 1	217.82	5.69	0.0015	(HOMO-22) → LUMO)	32.91 %
					(HOMO-2) → (LUMO)	22.59 %
					(HOMO -19) → (LUMO)	22.01 %
					(HOMO -18) → (LUMO)	47.15 %
	Band 2	217.69	5.69	0.0027	(HOMO) → (LUMO+1)	12.67 %
					(HOMO → LUMO)	35.22 %
					(HOMO) → (LUMO+3)	15.60 %
	Band 3	213.41	5.81	0.0006	(HOMO) → (LUMO)	51.83 %
					(HOMO -11) →(LUMO+1)	19.96 %
					(HOMO -9) →(LUMO+1)	15.79 %

Molecular Reactivity Analyses

The HOMO and LUMO are crucial chemical indicators largely used in this investigation. The maximum electronic charge (ΔN), electronic potential (μ), hardness (η), and global electrophilicity index (ω) as global indies of reactivity are calculated using the following equations [59–61]:

$\mu = 1 / 2 (E_{HOMO}+E_{LUMO})$ **(4)**

$\eta = 1 / 2 (E_{HOMO} - E_{LUMO})$ **(5)**

$\omega = \mu^2 / 2 \eta$ **(6)**

$ECT=(\Delta N \text{ max})_{host} -(\Delta N \text{ max})_{guest}$ **(7)**

Where $\Delta N(MAX)$host or guest = (-μ/ η) host or guest

The computed HOMO and LUMO energies and reactivity parameters of inclusion complexes in the gas phase and water calculated at CAM-B3LYP /6–G (d, p) are gathered in Table 3.

Table 3
HOMO, LUMO, gap (E_{HOMO}-E_{LUMO}), and the chemical reactive descriptors at the CAM- B3LYP /6–31 G (d,p) level calculations

	DMT	*β-CD*	Orientation A	Orientation B
In gas / in water				
HOMO (eV)	-8.19/ -8.38	-8.7 / -8.7	-8.299/ -8.381	-8.217/ -8.35
LUMO (eV)	1.06/ 0.979	2.45/ 2.748	0.952/ 0.925	0.517/ 0.571
gap (E_{LUMO}-E_{HOMO})(eV)	9.25/ 9.36	11.15/ 11.45	9.25/9.31	8.73/ 9.321
μ(eV)	− 3.56/- 3.70	-3.129/- 2.966	-3.74/ -3.728	-4.35/ -3.89
η(eV)	4.625/ 4.680	5.578/ 5.714	4.489/ 4.62	4.354/ 4.490
ω(eV)	1.36/ 1.44	0.87/ 0.7619	1.55/ 1.496	2.17/ 1.687
ΔN (MAX)	22.31/21.49	15.238/14.15	-	-
ECT	-	-	-7.07/-7.347	-7.07/-7.347

From Table 3, we noticed that t the HOMO-LUMO energy gap value in the water phase is 8.73 eV for Orientation A and 9.32 eV for Orientation B. The value of (E_{HOMO}- E_{LUMO}) gap for orientation B is higher than that of Orientation A, which indicates that Orientation B gives rise to a more stable complex than that of Orientation A. This result and the calculated binding energy are in good agreement.

The chemical potential of both orientations is negative, leading to a spontaneous inclusion process is spontaneous. $\mu_{free\ gues}$t $\mu_{free\ host}$; this indicates that the direction of the charge transfer associated with the creation of the inclusion complex is from DMT to β-C. We observed that the most significant value of chemical hardness (η) for model A is 4.62 eV in water; which is comparable to that of Orientation B (4.49 eV), indicating that the charge transfer in orientation B is significant. Additionally, compared to Orientation A, Orientation B exhibits a higher global electrophilicity index (ECT) value, indicating that charge transfer happens from the host to the guest. The result shows that orientation B corresponds to the most electrophilic complex.

Non Covalent Intermolecular Interactions

Natural bond orbital (NBO) analysis

The natural bonding orbital (NBO) analysis was obtained by means of the Gaussian 09 package at the CAM-B3LYP/6-31G(d, p) level [62–67].

These non-covalent interactions, in this case, result in the delocalization of electron density from a MO donor to a MO acceptor. They are described by second-order micro perturbations $E^{(2)}$ theory.

For each pair i (donor) and j (acceptor) the stabilization energy $E^{(2)}$ accompanying delocalization i→j is well defined in the literature [68, 69], which is given by the Eq. (8).

$$E^{(2)} = q_i F^2_{(i,j)}/(e_i - e_j)$$

8

qi is the donor orbital occupancy, εi and εj are diagonal elements, and F(i,j) is the off-diagonal NBO Fock matrix elements.

The stabilization energy $E^{(2)}$and bond length related to the most considerable interactions for complexes B identified by the CAM-B3LYP/6–31 G (d, p) method for B orientation in both gas and water phase are summarized in Table 4.

According to the results grouped in Table 4, two different classes of categories exist weak hydrogen formed between (LP) and (BD*) and Van der Waals interaction created between the (BD) and (BD*).

The higher stabilization second-order perturbation energy $E^{(2)}$ is 1.28 kcal/mol, associated with high donor-acceptor interaction corresponding to hydrogen bond length of 1.83 Å.

Accordingly, NBO calculations highlight the hydrogen bonds contribution sustaining the host-guest reaction and maintaining stability.

Table 4 NBO analysis of the second-order perturbation energies $E^{(2)}$ (Kcal/mol) of the hydrogen bond with CAM-B3LYP/6-31 G (d, p) for the B model

Donor	Acceptor	$E^{(2)}$ (kcal/mol)	H-bond (Å)
In vacuum			
DMT proton and β-CD acceptor			
BD (2) O 153 - C 156	BD*(1) O 74 - H 144	0.3	1.83
LP (1) O 153	BD*(1) O 74 - H 144	2.96	1.83
LP (2) O 153	BD*(1) O 74 - H 144	1.28	1.83
β-CD proton and DMT acceptor			
LP (1) O 63	BD* (1) C 158 - H 166	0.87	2.19
LP (2) O 63	BD* (1) C 158 - H 166	0.74	2.19
LP (1) O 66	BD* (1) N 154 - H 162	0.52	2.48
LP (1) O 75	BD* (1) C 159 - H 170	0.5	2.49
In water			
DMT proton and β-CD acceptor			
BD (2) O 153 - C 156	BD*(1) O 74 - H 144	0.31	1.83
LP (1) O 153	BD*(1) O 74 - H 144	2.97	1.83
LP (2) O 153	BD*(1) O 74 - H 144	1.35	1.83
β-CD proton and DMT acceptor			
LP (1) O 47	BD*(1) C 157 - H 164	0.76	2.25
LP (2) O 47	BD*(1) C 157 - H 164	0.47	2.25
LP (1) O 63	BD*(1) C 158 - H 166	0.85	2.19
LP (2) O 63	BD*(1) C 158 - H 166	0.77	2.19
LP (1) O 66	BD*(1) N 154 - H 162	0.51	2.49
LP (1) O 75	BD*(1) C 159 - H 170	0.5	2.49

BD denotes σ bonding orbital; DB* denotes σ* antibonding orbital, and LP corresponds to a lone pair.
BD denotes σ bonding orbital; DB* denotes σ* antibonding orbital, and LP corresponds to a lone pair.

Quantum Theory Of Atoms In Molecules (Qtaim)

The QTAIM analysis plays a crucial role in identifying intra- and intermolecular interactions. Quantum mechanical parameters such as electron density at the bond critical points (BBCPs) are used to determine the nature of host-guest interactions and classify bonding interactions [70].

The main topological parameters to define the properties of critical bond point BCPs are the total electron density ρ(r) and its Laplacian $\nabla^2\rho(r)$ [71–73].

In accord Bader's theory, the electron density ρ(r) and its Laplacian $\nabla^2\rho(r)$ should be positive at the H bond's critical points (+ 3, 1) and ranging from 0.002to 0.04 and from 0.024 to 0.139 for ρ(r) and $\nabla^2\rho(r)$ respectively (Fig. 6) [74].

The intermolecular bonding in the DMT@β -CD inclusion complexes is featured by the topological parameters: electron density (ρ), Laplacian of the electron density ($\nabla^2\rho$), kinetic energy densities G(r), the potential V(r), local electron energy densities H(r), the ratio of local gradient -G(R)/V(R), the bond energy E (E bond = V(r)/2) and eigenvalues (i) of Hessian (a.u) and ellipticity index ε (ε = $\lambda1/\lambda_2 - 1$) propounded by Espinosa [75].

Thus, Table 5 collects the QTAIM characterizing parameters of the (3, − 1) critical points of the DMT@β-CD complex. The QTAIM molecular graphs representing orientations B are illustrated in**Fig.5.**

The results gathered in Table 5, of the QTAIM calculation of model B using the CAM-B3LYP 6-31G(d, p) functional in gas and water shows an interaction between Dimethoate and β -CD through an H-bond.

As reported by Rozas et al. [76, 77], the interactions can be classified in accord with three types: (i), $\nabla^2\rho(r) < 0$ and H(r) < 0 are characteristics of strong covalent H bonds;(ii), medium H bonds with partial covalence are defined by $\nabla^2\rho(r) > 0$ and H(r) < 0, and (iii) the weak H bonds which are mainly of electrostatic when $\nabla^2\rho(r) > 0$ and H(r) > 0.

From CAM-B3LYP 6-31G(d, p) results, ρ (r) values, vary from 0.001 to 0.03 a.u and 0.001 to 0.029 a.u respectively for gas and water, while Laplacian $\nabla^2\rho(r)$ values are in the range 0.004- 0.094in gas and 0.0059 to 0.096a.u in water.

The results of ρ (r) in the gas phase and water showed values in the range of 0.001 to 0.03 a.u and of 0.001 to 0.029 a.u, respectively, with the corresponding Laplacian $\nabla^2\rho(r)$ varying between 0.004 and 0.094 a.u in the gas phase and 0.0059 and 0.096 a.u in water.

However, stronger hydrogen bonding O153—H144 is observed with the lowest intermolecular distance of 1.83Á in the gas and aqueous phase and the maximum electron density ρ(r) and Laplacian $\nabla^2\rho(r)$.

The ellipticity values for the intermolecular bonding of the DMT@β-CD complex range from 0.002 to 1.23 a.u in gas and from 0.02 to 0.23a.u in water, indicating stable contact between the host and guest[78].

All calculated $\nabla^2\rho(r)$ and H(r) values are positive, indicating the presence of weak electrostatic interactions and the calculated ratio of -G(r)/V(r) is > 1, relative to significant interactions of the non-covalent character.

The topological parameters Table 5 in the gas phase and water, display all H(r) values are positive and $\nabla^2\rho(r)$ are all small positive values implying weak interaction mainly of electrostatic. Besides, the ratio of−G(r)/V(r) is > 1 for the complex, supporting the existence of weak intermolecular bonding. The Table 5 bond energy (E) values show that the principal molecular interaction in the gas phase or water is detected for O153—H144 with − 0.011 kcal/mol.

The result of 1, 2, and 3, corresponding to the Hessian eigenvalues of the electron density at BCP, indicates that 1 2 3, the sum of negative curvatures (1 + 2) as well as the positive, while (3) decreases with H···O distances.

This result shows that the electron density increase in the plane perpendicular to the bond path occurs concurrently with electron density depletion along the bond path. Lower ellipticity index values demonstrate that electrons are delocalized through the associated atoms.

The QTAIM results show that van der Waals interactions and weak hydrogen bonds are the chief factors influencing the complex's stability.

Hydrogen bond distance, topological parameters in (au): electron density ρ(r), Laplacian of electron density $\nabla^2\rho(r)$. Energetic topological parameters in (kcal/mol): electron kinetic energy density G (r), electron potential energy density V (r), total electron energy density H (r).

NCI- RDG analysis

In order to identify hydrogen bonds, van der Waals contacts, and repulsive steric interactions between host and guest in the formed complex, the non-covalent interaction (NCI) via a reduced density gradient (RDG) was employed [79, 80].

The equation that describes the RDG approach is as follows [79]:

$$RDG(r) = 1|\nabla\rho(r)|/\ 2(3\pi2)^{1/3}\rho(r)^{4/3} \quad \textbf{(9)}$$

Consider Fig. 7a, which plots RDG against sign (λ_2) ρ; the sign (λ_2) value can be used to indicate the type of interaction; for example, sign (λ_2) > 0 indicates a repulsive interaction, while sign (λ_2) < 0 indicates an attractive interaction, such as hydrogen bonds.

It is observed that van der Waals interactions are ranged from − 0.018 to 0.005 a.u and are shown with a green spot; the hydrogen bonding interactions are illustrated with a blue spot and located between − 0.05 and − 0.02 a.u. The red spot indicates the repulsive steric forces.

From the 3D spatial NCI isosurface diagram (Fig. 7b), we can see that there are critical green patches in the region between DMT and β-CD related to van der Waals interactions, indicating that the guest forms a stable inclusion complex with the host. Besides, a blue patch represents the strong hydrogen bonding interactions and red spots represent the repulsive steric forces.

IGM analysis

The independent gradient model (IGM) quantifies the intermolecular interactions between DMT and β-CD to determine their nature, which can be supplied by δginter and δgintra [81].

Figure 8 illustrates the IGM isosurfaces of δ_{ginter} and δ_{gintra} versus sign(λ_2) ρ (for DMT@β-CD studied complex. The resulting 2-D scatter plot shows that red points correspond to δ_{ginter}, while black points represent δ_{gintra}.

Figure 8, with the most intense black peak appearing on the negative side at sign(λ_2)ρ =-0.28 with δ_{ginter} of 0.392 au. Van der Waals interactions can be seen in the region where sign(λ_2)ρ=-0.04, with δ_{ginter} of approximately 0.056 au corresponding at the second less intense peak. In contrast, the positive side of the sign(λ_2)ρ peak lies in the range of 0.04 to 2.00 with δ_{ginter} = 0.168au, indicating a repulsive interaction.

The 3-D IGM isosurface map for encapsulated complexes is depicted in Fig. 8. The green-colored regions represent weak van der Waals interactions, whereas blue regions denote stronger electrostatic attraction. The results show that the DMT@β-CD complex is stabilized by hydrogen bonds and van der Waals interactions. From these results, it can be concluded that there are intermolecular hydrogen bonds, and the IGM analysis is in good agreement with the QTAIM results.

Energy decomposition analysis (EDA)

To highlight and evaluate the hydrogen bonding between DMT and β-CD in gas and aqueous phases, the Morokuma and Ziegler-Rauk energy decomposition analysis (EDA) [83–85] was applied, which was widely used previously [86–93]. Thus, the EDA using the hybrid B3LYP-D3 functional gives rise to the resulting interaction energy ΔEint which is decomposed into four terms of energy as given below: the electrostatic interaction ΔEelstat which is an attractive interaction, the Pauli interaction ΔEPauli that exhibits a repulsive interaction, the orbital interaction ΔEorb as an attractive term refers to the charge transfer between the occupied orbitals and the unoccupied orbitals of the two fragments and finally ΔEdisp corresponding to the Grimme dispersion correction term.

Table 5 Topological parameters computed by QTAIM for model B of DMT@β-CD complex

	d(Å)	$\rho(r)$	$\nabla^2\rho(r)$	λ_1	λ_2	λ_3	$\rho(r)$	G(r)	V(r)	H(r)	-G(r)/V(r)	E_{HB}
In aqueous phase												
110(H) – 152(O)	2.518	0.00903	0.0298	-0.0092	-0.00858	0.047	0.0738	0.00686	-0.00626	0.00059	1.096	-0.0031
102(H) – 160(H)	2.778	0.00184	0.0059	-0.00139	-0.00129	0.0086	0.0801	0.0010	-0.00065	0.0004	1.5386	-0.0003
66(O) - - 162(H)	2.39	0.0099	0.0312	-0.011	-0.010	0.05	0.0335	0.0075	0.0073	0.0002	1.0276	-0.0036
100(H) – 154(N)	2.958	0.004	0.015	-0.004	-0.002	0.022	0.548	0.003	-0.002	0.0008	1.5	-0.001
59(O) - - 169(H)	2.712	0.006	0.021	-0.0059	-0.005	0.0326	0.0667	0.004	-0.003	0.0008	1.33	-0.0015
161(H) – 90(H)	2.754	0.002	0.0064	-0.0015	-0.0014	0.0094	0.1025	0.0011	-0.0007	0.0004	1.571	-0.0003
170(H) – 75(O)	2.678	0.0063	0.0216	-0.006	-0.006	0.034	0.051	0.0046	-0.0039	0.0007	1.179	-0.0019
153(O) – 121(H)	2.499	0.0099	0.0329	-0.0094	-0.0077	0.050	0.233	0.0075	-0.0067	0.00075	1.119	-0.0033
153(O) – 144(H)	1.827	0.0299	0.096	-0.0411	-0.0403	0.1776	0.0199	0.0231	-0.0222	0.00087	1.040	-0.0111
153(O) – 81(H)	2.723	0.0055	0.0198	-0.0049	-0.0046	0.029	0.0632	0.0041	-0.0033	0.00079	1.242	-0.001
In gas phase												
102(H) – 160(H)	2.98	0.0013	0.0040	-0.00090	-0.00071	-0.71	0.0026	0.0072	-0.0045	0.00027	1.6	-0.0022
59(O) - - 169(H)	2.75	0.0056	0.0197	-0.0054	-0.005	0.03	0.0776	0.0041	-0.0033	0.0008	1.242	-0.0016
100(H) – 154(N)	2.95	0.00479	0.0145	-0.0040	-0.0029	0.021	0.3823	0.00298	-0.0023	0.00064	1.2956	-0.0011
107(H) – 169(H)	2.85	0.0024	0.00791	-0.0015	-0.00108	0.0105	0.3973	0.00149	-0.001	0.00047	1.49	-0.0005
161(H) – 90(H)	2.679	0.0025	0.0081	-0.0020	-0.00178	0.0119	0.1313	0.00149	-0.0009	0.00053	1.5684	-0.00047
157(C) – 52(H)	2.98	0.0040	0.0156	-0.0021	-0.00096	0.0187	1.231	0.00296	-0.0020	0.00095	1.48	-0.001
170(H) – 75(O)	2.49	0.0093	0.029	-0.00984	-0.00925	0.0483	0.0637	0.0068	-0.0064	0.00046	1.064	-0.00319
153(O) – 121(H)	2.569	0.0087	0.0296	-0.008	-0.0061	0.0438	0.303	0.0065	-0.0056	0.00086	1.1607	-0.0028
164(H) –	2.25	0.015	0.0436	-0.0176	-0.0166	0.0779	0.064	0.0112	-0.0115	-0.0003	0.974	-0.0057

47(O)												
153(O) – 144(H)	1.835	0.0292	0.094	-0.040	-0.0389	0.173	0.03	0.0227	-0.0218	0.00088	1.041	-0.0109
153(O) – 81(H)	2.655	0.00638	0.022	-0.0059	-0.0056	0.0337	0.049	0.0047	-0.004	0.00077	1.175	-0.002

$$\Delta E_{int} = \Delta E_{elstat} + \Delta E_{Pauli} + \Delta E_{orb+} \Delta E_{Disp} \quad (10)$$

$$\Delta E_{elestat(\%)} = \Delta E_{orb} / (\Delta E_{orb} + \Delta E_{elestat} + \Delta E_{disp}) \times 100 \quad (11)$$

$$\Delta E_{orb(\%)} = \Delta E_{orb} / (\Delta E_{orb} + \Delta E_{elestat} + \Delta E_{disp}) \times 100 \quad (12)$$

$$\Delta E_{disp(\%)} = \Delta E_{orb} / (\Delta E_{orb} + \Delta E_{elestat} + \Delta E_{disp}) \times 100 \quad (13)$$

The ΔE_{int} energies gathered in the Table 6 are negative indicating stabilization effects of these interactions. The analysis of the results shows that the interaction energy of -43.88 kcal/mol in gas phase is upper than that obtained in water phase of -70.2 kcal/mol. The divergence between the two values comes essentially from the ΔE_{Pauli}, ΔE_{elstat} and ΔE_{orb} contributions into the ΔE_{int} total interaction energy, where the former is considerably weakened, whereas the two later terms are substantially strengthened (increased absolute values) as summarized in Table 6. Indeed, the ΔE_{orb} goes up from 20 to 35% and increases from 4à to 44%. Besides, the contribution is not influenced by the change middle – 34.73 *vs* -33.88 kcal/mol. The ΔE_{disp} relative to the hydrogen interactions contributes by 39.12% in gas and 31.77% in water into the total interaction energy. Thus, put emphasis on strong hydrogen interaction type between DMT and β-CD.

The ΔE_{Pauli} energy identifies the steric repulsion between the fragments. However, in Table 6, the ΔE_{Pauli} energies of the complex ranging from 44.90 to 39.85 kcal/mol in gas and water, respectively, which are compensated by the sum of the electrostatic, the orbital and dispersion stabilization terms, however, this destabilization is reduced in the presence of water.

Table 6
Energetic contribution from an energy decomposition analysis

	2B(gas)	2B (water)
$\Delta E_{bonding}$	-43.88	-70.91
ΔE_{pauli}	44.90	36.85
$\Delta E_{elestat}$	-35.99	-48.03
ΔE_{orb}	-18.06	-25.85
ΔE_{disp}	-34.73	-33.88
ΔE_{orb} (%)	20.34	23.99
$\Delta E_{elestat}$ (%)	40.54	44.57
ΔE_{disp} (%)	39.12	31.44

Conclusion

This theoretical reports the interactions between DMT and β-CD in gas and aqueous phases. The results obtained indicated that orientation B is more privileged than that of A one in both cases, where the optimized structures of the DMT@β-CD complex confirms the total inclusion of dimethoate into the β-CD cavity. NBO results revealed that the guest molecule interacts with the host and modifies its charge distribution to form a stable inclusion complex. QTAIM, NBO and EDA analyses confirm the existence of hydrogen bonds between β-cyclodextrin and dimethoate. RDG and IGM calculations showed that DMT@β-CD forms a combination of weak hydrogen bonds and van der Waals interactions which stabilizes the complex. NCI isosurface confirms the establishment of hydrogen bonds and vdW and steric repulsion during inclusion complex formation. Considering the inclusion of dimethoate in β -cyclodextrin, this study could serve as a starting point for experiments on pesticide environmental problems.

Declarations

Acknowledgments

This study was supported by the HPC resources of UCI-UFMC (Unité de Calculintensif of the University Freres Mentouri Constantine 1).

Ethical approval

This chapter does not contain any studies with human participants or animals performed by any of the authors.

Competing interests

The authors declare no competing interests.

Author's contributions

Amina Benaissa: Data curation, writing original draft; Abdelaziz Bouhadiba: Investigation and supervision; Noura Naili, and Faiza Chekkal: performed the theoretical calculation, conceptualization, methodology, software; Malika Khelfaoui, Bouras Ibtissem, Mehri Karima: data analysis and contributed to the manuscript preparation; Mohamed Salah Madjram, Bachir Zouchoune: supervision, calculations, validation and editing; Sulaiman Mogalli, Najran Malfi: conceptualization, formal analysis, writing-review; Leila Nouar, Fatiha Madi: advising and writing-review and editing.

The manuscript was written through contribution of all authors. All authors have given approval to the final version of the manuscript.

Conflict of interest the authors declare they have no conflict of interest.

References

1. Schäfer RB (2019) Responses of freshwater macroinvertebrates to pesticides: insights from field studies. Curr Opin Environ Sci Health 11: 1 7.
2. Trokhymenko GG, Grushyna OG, Marynets OM, Blahodatnyi VV (2022) Study of Harmful Effects of Pesticides, Especially Seed Producers, on the Components of Agrocenosis. EEET 23
3. Liess M, Liebmann L, Vormeier P, Weisner O, Altenburger R, Borchardt D et al (2021) Pesticides are the dominant stressors for vulnerable insects in lowland streams. Water Res 201: 117262
4. Schneeweiss A, Schreiner VC, Reemtsma T, Liess M, Schäfer RB (2022) Potential propagation of agricultural pesticide exposure and effects to upstream sections in a biosphere reserve. Sci Total Environ 836: 155688
5. Weisner O, Arle J, Liebmann L, Link M, Schäfer RB, Schneeweiss A et al (2022) Three reasons why the Water Framework Directive (WFD) fails to identify pesticide risks. Water Res 208: 117848
6. Le TDH, Scharmüller A, Kattwinkel M, Kühne R, Schüürmann G, Schäfer RB (2017) Contribution of waste water treatment plants to pesticide toxicity in agriculture catchments. Ecotoxicol Environ Saf 145: 135 141
7. Le Cor F, Slaby S, Dufour V, Iuretig A, Feidt C, Dauchy X, Banas D (2021) Occurrence of pesticides and their transformation products in headwater streams: Contamination status and effect of ponds on contaminant concentrations. Sci Total Environ 788 : 147715
8. Vonk JA, Kraak MH (2020) Herbicide exposure and toxicity to aquatic primary producers. Rev Environ Contam Toxicol 250: 119 171
9. Spilsbury FD, Warne MSJ, & Backhaus T (2020) Risk assessment of pesticide mixtures in Australian rivers discharging to the Great Barrier Reef. J Environ Sci Technol 54(22): 14361 14371
10. Singh NS, Sharma R, Parween T, Patanjali PK (2018) Pesticide contamination and human health risk factor. In Modern age environmental problems and their remediation (pp. 49-68). Springer, Cham
11. Singh P, Prasad SM (2018) Antioxidant enzyme responses to the oxidative stress due to chlorpyrifos, dimethoate and dieldrin stress in palak (Spinacia oleracea L.) and their toxicity alleviation by soil amendments in tropical croplands. Sci Total Environ 630: 839 848
12. Bonnechère A, Hanot V, Jolie R, Hendrickx M, Bragard C, Bedoret T,Van Loco J (2012) Effect of household and industrial processing on levels of five pesticide residues and two degradation products in spinach. Food Control 25(1): 397 406
13. Eto M, Zweig G (2018) Organophosphorus pesticides: organic and biological chemistry. CRC press
14. Abdelghany EM, Amira EA, Hassan H (2019) Beneficial effect of quercetin against dimethoate induced cerebellar cortex injury in adult male albino rat: histological and immunohistochemical study. Med J Cairo Univ 87(December): 5121 5134
15. Singh RN, Pandey RK, Singh NN, Das VK (2009) Acute toxicity and behavioral responses of common carp Cyprinus carpio (Linn.) to an organophosphate (Dimethoate). WJZ 4(2): 70 75
16. Mahalapbutr P, Wonganan P, Charoenwongpaiboon T, Prousoontorn M, Chavasiri W, Rungrotmongkol T (2019) Enhanced solubility and anticancer potential of mansonone G by β-cyclodextrin-based host-guest complexation: A computational and experimental study. Biomolecules 9(10): 545
17. Waris KH, Lee VS, Mohamad S (2021) Pesticide remediation with cyclodextrins: a review. ESPR 28(35): 47785 47799
18. Sikder MT, Rahman MM, Jakariya M, Hosokawa T, Kurasaki M, Saito T (2019) Remediation of water pollution with native cyclodextrins and modified cyclodextrins: A comparative overview and perspectives. J Chem Eng 355: 920 941
19. Martin J, Díaz-Montaña E J, Asuero AG (2018) Cyclodextrins: past and present. Cyclodextrin: A Versatile Ingredient; Arora, P., Dhingra, N., Eds, 1-43

20. Tafazzoli M, Ghiasi M (2009) Structure and conformation of α-, β-and γ-cyclodextrin in solution: Theoretical approaches and experimental validation. Carbohydr Polym 78(1): 10 15
21. Meryem G, Rabah K, Fatiha M, Leila N, Aziz BA, Imane D, Rachid M (2021) Computational investigation of vanillin@ βéta-cyclodextrin inclusion complex: Electronic and intermolecular analysis. J Mol Liq 321: 114839
22. Rayene K, Imane D, Abdelaziz B, Leila N, Fatiha M, Abdelkrim G et al (2022) Molecular modeling study of structures, Hirschfield surface, NBO, AIM, RDG, IGM and 1HNMR of thymoquinone/hydroxypropyl-β-cyclodextrin inclusion complex from QM calculations. J Mol Struct 1249: 131565
23. Veiga MD, Díaz PJ, Ahsan F (1998) Interactions of griseofulvin with cyclodextrins in solid binary systems. J Pharm Sci 87(7): 891 900
24. Li J, Loh XJ (2008) Cyclodextrin-based supramolecular architectures: syntheses, structures, and applications for drug and gene delivery. Adv Drug Deliv Rev 60(9): 1000 1017
25. Cal K, Centkowska K(2008) Use of cyclodextrins in topical formulations: Practical aspects. Eur. J. Pharm. Biopharm 68(3): 467 478
26. Assaba IM, Rahali S, Belhocine Y, Allal H (2021) Inclusion complexation of chloroquine with α and β-cyclodextrin: Theoretical insights from the new B97-3c composite method. J Mol Struct 1227:129696
27. Bogdan M, Floare CG, Buimaga-Iarinca L, Morari C, Pirnau A (2016) NMR study and computational assays of meclofenamic Na salt and β-cyclodextrin inclusion complex. J Incl Phenom Macrocycl Chem 85(1): 111 -120
28. Ikeda Y, Motoune S, Marumoto A, Sonoda Y, Hirayama F, Arima H, Uekama K (2002) Effect of 2-hydroxypropyl-β-cyclodextrin on release rate of metoprolol from ternary metoprolol/2-hydroxypropyl-β-cyclodextrin/ethylcellulose tablets. J Incl Phenom Macrocycl Chem 44(1): 141 144
29. Safia H, Ismahan L, Abdelkrim G, Mouna C, Leila N, Fatiha M (2019) Density functional theories study of the interactions between host β-cyclodextrin and guest 8-anilinonaphthalene-1-sulfonate: Molecular structure, HOMO, LUMO, NBO, QTAIM and NMR analyses. J Mol Liq 280: 218 229
30. Nora M, Ismahan L, Abdelkrim G, Mouna C, Leila N, Fatiha M et al (2020) Interactions in inclusion complex of β-cyclodextrin/l-Metheonine: DFT computational studies. J Incl Phenom Macrocycl Chem 96(1): 43 54
31. Rahali S, Belhocine Y, Allal H , Bouhadiba A, Assaba IM, Seydou M (2022) A DFT investigation of the host–guest interactions between boron-based aromatic systems and β-cyclodextrin. J Struct Chem 33(1): 195 206
32. Prabhu A, Fatiha M, Leila N, Raj TA, Navarro-González I, Periago MJ et al (2018). Investigation of 3D Contour Map and Intermolecular Interaction of Dopamine with β-Cyclodextrin and 2-Hydroxypropyl-β-cyclodextrin. J Solution Chem 47(3): 409 429
33. Gaussian09, Frisch MJ, Trucks GW, Schlegel HB, Scuseria GE, Robb MA, Cheeseman JR, Scalmani G, Barone V, Mennucci B, Petersson GA, Nakatsuji H, Caricato M, Li X, Hratchian HP, Izmaylov AF, Bloino J, Zheng G, Sonnenberg JL, Hada M, Ehar M (2009) Inc Wallingford CT 121:150 166
34. Dennington R, Keith T, Millam J (2009) Semichem Inc. Shawnee Mission KS, GaussView, Version, 5
35. Bolton EE, Wang Y, Thiessen PA, Bryant S H (2008) PubChem integrated platform of small molecules and biological activities. In Annual reports in computational chemistry (Vol. 4, pp. 217-241). Elsevier
36. Chem-Office 3D ultra, (2006) Version 10, Cambridge Software
37. MOPAC, James JP, Stewart (2016) Stewart Computational Chemistry, Colorado Springs. CO, USA http://OpenMOPAC.net
38. Hyperchem (2002) Release 7.51 for Windows, Hypercube Inc.,. Hyperchem 7.5
39. Chermette H (1998) Density functional theory: a powerful tool for theoretical studies in coordination chemistry. Coord Chem Rev 178: 699 721
40. Andrews L, Citra A (2002) Infrared spectra and density functional theory calculations on transition metal nitrosyls. Vibrational frequencies of unsaturated transition metal nitrosyls. Chem Rev 102(4): 885 912
41. Ziegler T, Autschbach J (2005) Theoretical methods of potential use for studies of inorganic reaction mechanisms. Chem Rev 105(6): 2695 2722
42. Schultz NE, Zhao Y, Truhlar DG (2005) Density functionals for inorganometallic and organometallic chemistry. J Phys Chem A 109(49): 11127 11143
43. Zhao Y, Truhlar DG (2008) The M06 suite of density functionals for main group thermochemistry, thermochemical kinetics, noncovalent interactions, excited states, and transition elements: two new functionals and systematic testing of four M06-class functionals and 12 other functionals. Theor Chem Acc 120(1): 215 241
44. Grimme S, Antony J, Ehrlich S, Krieg H (2010). A consistent and accurate ab initio parametrization of density functional dispersion correction (DFT-D) for the 94 elements H-Pu. J Chem Phys 132(15): 154104
45. Torres E, DiLabio GA (2012) A (nearly) universally applicable method for modeling noncovalent interactions using B3LYP. J. Phys Chem Lett 3(13): 1738-1744
46. Soniat M, Rogers DM, Rempe SB (2015) Dispersion-and exchange-corrected density functional theory for sodium ion hydration. J Chem Theory Comput 11(7): 2958 2967
47. DiLabio GA, Johnson ER, Otero-de-la-Roza A (2013) Performance of conventional and dispersion-corrected density-functional theory methods for hydrogen bonding interaction energies. Phys Chem Chem Phys 15(31): 12821 12828

48. Cossi M, Rega N, Scalmani G, Barone V (2003) Energies, structures, and electronic properties of molecules in solution with the C-PCM solvation model. J Comput Chem 24(6): 669 681
49. Leila N, Sakina H, Bouhadiba A, Madi F (2011) Theoretical study of inclusion complexation of 3-amino-5-nitrobenzisothiazole with β-cyclodextrin. J Mol Liq 160(1): 8 13
50. Nora M, Fatiha M, Leila N, Sakina H, DjamelEddine K (2015) Density functional study of inclusion complex of Albendazole/cucurbit [7] uril: Structure, electronic properties, NBO, GIAO and TD-DFT analysis. J Mol Liq 211: 40 -47
51. Leila N, Sakina H, Bouhadiba A, Fatiha M, Leila L (2011) Molecular modeling investigation of para-nitrobenzoic acid interaction in β-cyclodextrin. J Mol Liq 160(1): 1 7
52. Alvira E, Mayoral JA, Garcia JI (1997) Molecular modelling study of β-cyclodextrin inclusion complexes. Chem Phys Lett 271(1-3):178 184
53. Haiahem S, Nouar L, Djilani I, Bouhadiba A, Madi F, Khatmi DE (2013) Host-guest inclusion complex between β-cyclodextrin and paeonol: A theoretical approach. C R Chim 16(4): 372 379
54. Glendening ED, Landis CR, Weinhold F (2012) Natural bond orbital methods. Wiley Interdiscip Rev Comput Mol Sci 2(1): 1 42
55. Shukla M, Srivastava N, Saha S (2012) Investigation of ground state charge transfer complex between paracetamol and p-chloranil through DFT and UV–visible studies. J Mol Struct 1021: 153 157
56. Lu T, Chen F (2012) Multiwfn: a multifunctional wavefunction analyzer. J Comput Chem 33(5) : 580 592
57. Humphrey W, Dalke A, Schulten K (1996) VMD: visual molecular dynamics. J Mol Graph 14(1): 33 38
58. Saha S, Roy A, Roy K, Roy MN (2016) Study to explore the mechanism to form inclusion complexes of β-cyclodextrin with vitamin molecules. Sci Rep 6(1): 1 12
59. Chen F, Wang Y, Xie X, Chen M, Li W (2014) TDDFT study of UV–vis spectra of permethrin, cypermethrin and their beta-cyclodextrin inclusion complexes: A comparison of dispersion correction DFT (DFT-D3) and DFT. Spectrochim Acta A Mol Biomol Spectrosc 128: 461 467
60. Geerlings P, De Proft F, Langenaeker W (2003) Conceptual density functional theory. Chem Rev 103(5): 1793 1874
61. Parr RG, Pearson RG (1983) Absolute hardness: companion parameter to absolute electronegativity. J Am Chem Soc 105(26): 7512 7516
62. Parr RG, Szentpály LV, Liu S (1999) Electrophilicity index. J Am Chem Soc 121(9): 1922 1924
63. Suvitha A, Venkataramanan NS (2017) Trapping of organophosphorus chemical nerve agents by pillar [5] arene: A DFT, AIM, NCI and EDA analysis. J Incl Phenom Macrocycl 87(1): 207 218
64. Reed AE, Curtiss LA, Weinhold F (1988) Intermolecular interactions from a natural bond orbital, donor-acceptor viewpoint. Chem Rev 88(6): 899 926
65. Prabhu MD, Yenagi JT, Kamat V, Tonannavar J (2020) XRD structure and vibrational analysis of DL-β-Leucine, as aided by DFT tetramer model and characterized by NBO, AIM and NCI calculations. J Mol Struct 1218: 128495
66. Madhu DK, Madhavan J (2018) Quantum chemical analysis of electronic structure and bonding aspects of choline based ionic liquids. J Mol Liq 249: 637 649
67. Zarie-Moghaddam E, Zahedi-Tabrizi M (2019) QTAIM, NBO, and NMR studies of hydrogen bonds in capecitabine. Monatsh fur Chem 150(7): 1267 1274
68. Suvitha A, Venkataramanan NS, Sahara R, Kawazoe Y (2019) A theoretical exploration of the intermolecular interactions between resveratrol and water: a DFT and AIM analysis. J Mol Model 25(3): 1 11
69. Weinhold F, Landis CR, Glendening ED (2016) What is NBO analysis and how is it useful?. Int Rev Phys Chem 35(3): 399 440
70. Rezaei-Sameti M, Zarei P (2018) NBO, AIM, HOMO–LUMO and thermodynamic investigation of the nitrate ion adsorption on the surface of pristine, Al and Ga doped BNNTs: A DFT study. Adsorption 24(8): 757 767
71. Venkataramanan NS, Suvitha A, Kawazoe Y (2017) Intermolecular interaction in nucleobases and dimethyl sulfoxide/water molecules: A DFT, NBO, AIM and NCI analysis. J Mol Graph 78: 48 60
72. Bader RF (2006) Comment on: Revisiting the variational nature of the quantum theory of atoms in molecules. Chem Phys Lett 426(1 3): 226 228
73. Becke A (2007) The quantum theory of atoms in molecules: from solid state to DNA and drug design. John Wiley & Sons
74. Kumar PSV, Raghavendra V, Subramanian V (2016) Bader's theory of atoms in molecules (AIM) and its applications to chemical bonding. Chem Sci J 128(10): 1527 1536
75. Bader RF (1985) Atoms in molecules. Acc Chem Res 18(1): 9 15
76. Espinosa E, Molins E, Lecomte C (1998) Hydrogen bond strengths revealed by topological analyses of experimentally observed electron densities. Chem Phys Lett 285(3 4): 170 173.
77. Rozas I, Alkorta I, Elguero J (2000) Behavior of ylides containing N, O, and C atoms as hydrogen bond acceptors. J Am Chem Soc 122(45): 11154 11161
78. Alkorta I, Rozas I, Elguero J (2002) Theoretical study of the Si–H group as potential hydrogen bond donor. Int J Quantum Chem 86(1) 122 129

79. Venkataramanan NS, Suvitha A, Kawazoe Y (2018) Unravelling the nature of binding of cubane and substituted cubanes within cucurbiturils: A DFT and NCI study. J Mol Liq 260: 18 29
80. Sahu D, Jana K, Ganguly B (2017) The role of non-covalent interaction for the adsorption of CO 2 and hydrocarbons with per-hydroxylated pillar [6] arene: a computational study. New J Chem 41(20): 12044 12051
81. Zahed E, Shaabani S, Shiroudi A (2017) Following the molecular mechanism of decarbonylation of unsaturated cyclic ketones using bonding evolution theory coupled with NCI analysis. J Phys Chem A 121(44) 8504 8517
82. Lefebvre C, Rubez G, Khartabil H, Boisson JC, Contreras-García J, Henon E (2017) Accurately extracting the signature of intermolecular interactions present in the NCI plot of the reduced density gradient versus electron density. Phys Chem Chem Phys 19(27): 17928 17936
83. Morokuma K (1971) Molecular orbital studies of hydrogen bonds. III. C= O··· H–O hydrogen bond in H2CO··· H2O and H2CO··· 2H2O. J Chem Phys 55(3) : 1236 1244
84. Ziegler T, Rauk A (1979) Carbon monoxide, carbon monosulfide, molecular nitrogen, phosphorus trifluoride, and methyl isocyanide as. sigma. donors and. pi. acceptors. A theoretical study by the Hartree-Fock-Slater transition-state method. Inorg Chem 18(7) : 1755 1759
85. Ziegler T, Rauk A (1979) A theoretical study of the ethylene-metal bond in complexes between copper (1+), silver (1+), gold (1+), platinum (0) or platinum (2+) and ethylene, based on the Hartree-Fock-Slater transition-state method. Inorg Chem 18(6): 1558 1565
86. Khireche M, Zouchoune B, Ferhati A, Nemdili H, Zerizer MA (2021) Understanding the chemical bonding in sandwich complexes of transition metals coordinated to nine-membered rings: energy decomposition analysis and the donor–acceptor charge transfers. Theor Chem Acc 140(9): 1 17
87. Frenking G, Froehlich N (2000) The nature of the bonding in transition-metal compounds. Chem Rev 100(2): 717 774
88. Tabrizi L, Zouchoune B, Zaiter A (2020). Theoretical and experimental study of gold (III), palladium (II), and platinum (II) complexes with 3-((4-nitrophenyl) thio) phenylcyanamide and 2, 2'-bipyridine ligands: cytotoxic activity and interaction with 9-methylguanine. Inorganica Chim Acta 499 : 119211
89. Tabrizi L, Zouchoune B, Zaiter A (2019) Experimental and theoretical investigation of cyclometallated platinum (ii) complex containing adamantanemethylcyanamide and 1, 4-naphthoquinone derivative as ligands: synthesis, characterization, interacting with guanine and cytotoxic activity. RSC Adv 9(1): 287 300
90. Mokrane Z, Zouchoune B, Zaiter A (2020) Coordination's preference and electronic structure of N-heterocyclic carbene–monometallic complexes: DFT evaluation of σ-bonding and π-backbonding interactions. Theor Chem Acc 139(7): 1 14
91. Zaiter A, Zouchoune B (2018) Electronic structure and energy decomposition of binuclear transition metal complexes containing β-diketiminate and imido ligands: spin state and metal's nature effects. Struct Chem 29(5): 1307 1320
92. Zerizer MA, Nemdili H, Zouchoune B (2022) Electron transfers' assessment between stannol ring of triple-decker complexes and M (CO) 5 (M= Cr, Mo, W), MnCp (CO) 2 and CoCp (CO) metallic fragments: Bonding and energy decomposition analysis. Polyhedron 223: 115960
93. Mecheri S, Zouchoune B, Zendaoui SM (2020) Bonding and electronic structures in dinuclear (X)[(Ind) M2L2] complexes (M= Ni, Pd, L= CO, PEt3, X= Cl, Allyl, Ind= indenyl, Cp= cyclopentadienyl): analogy between four-electron donor ligands. Theor Chem Acc 139(1): 1 13

Figures

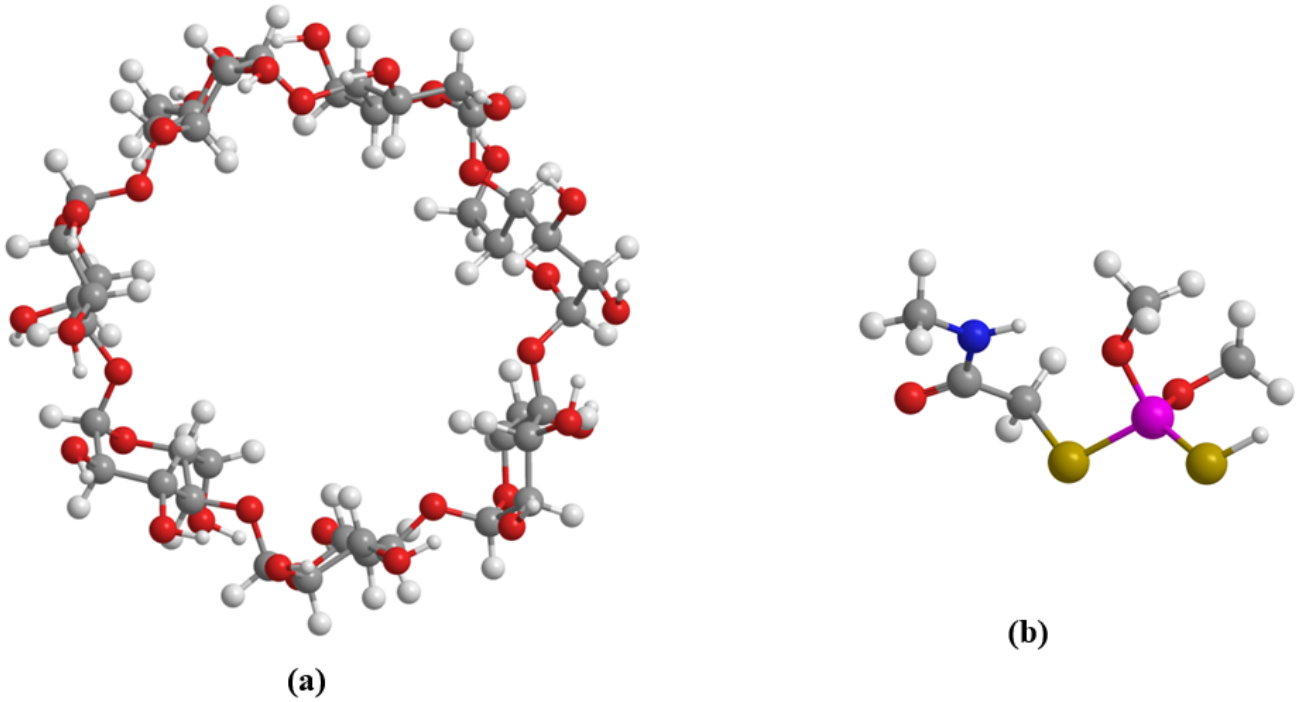

Figure 1

Molecular structures of β-CD (a) and Dimethoate (b)

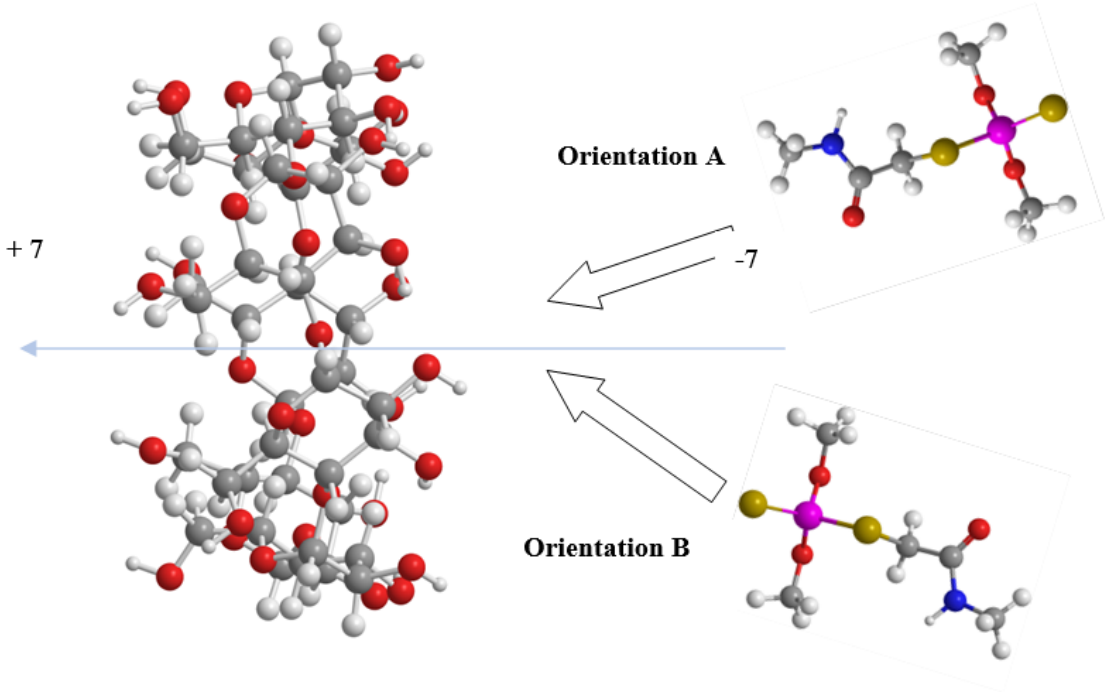

Figure 2

The complexation process for A and B models

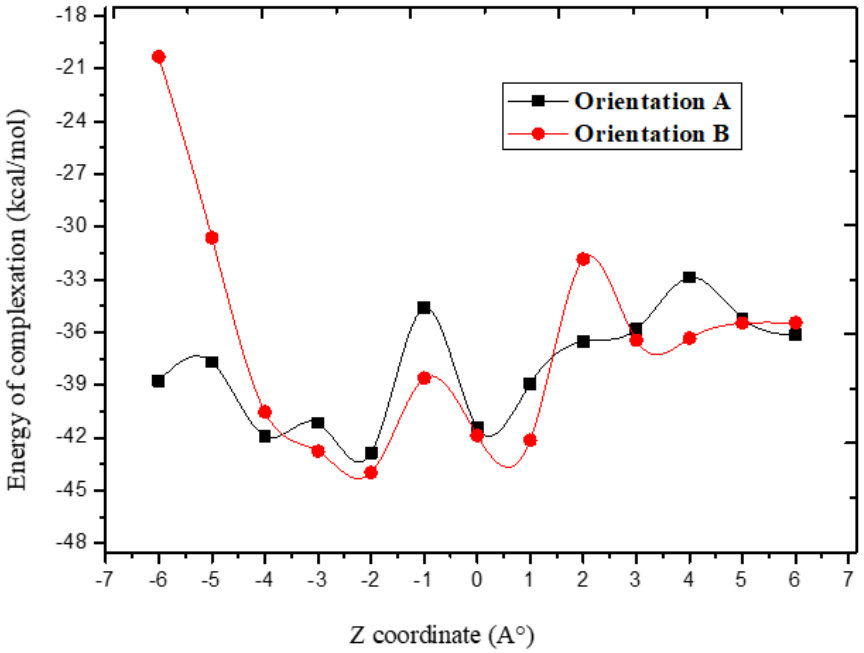

Figure 3

Variation of the inclusion complexation of dimethoate into β-CD obtained by PM7 calculations

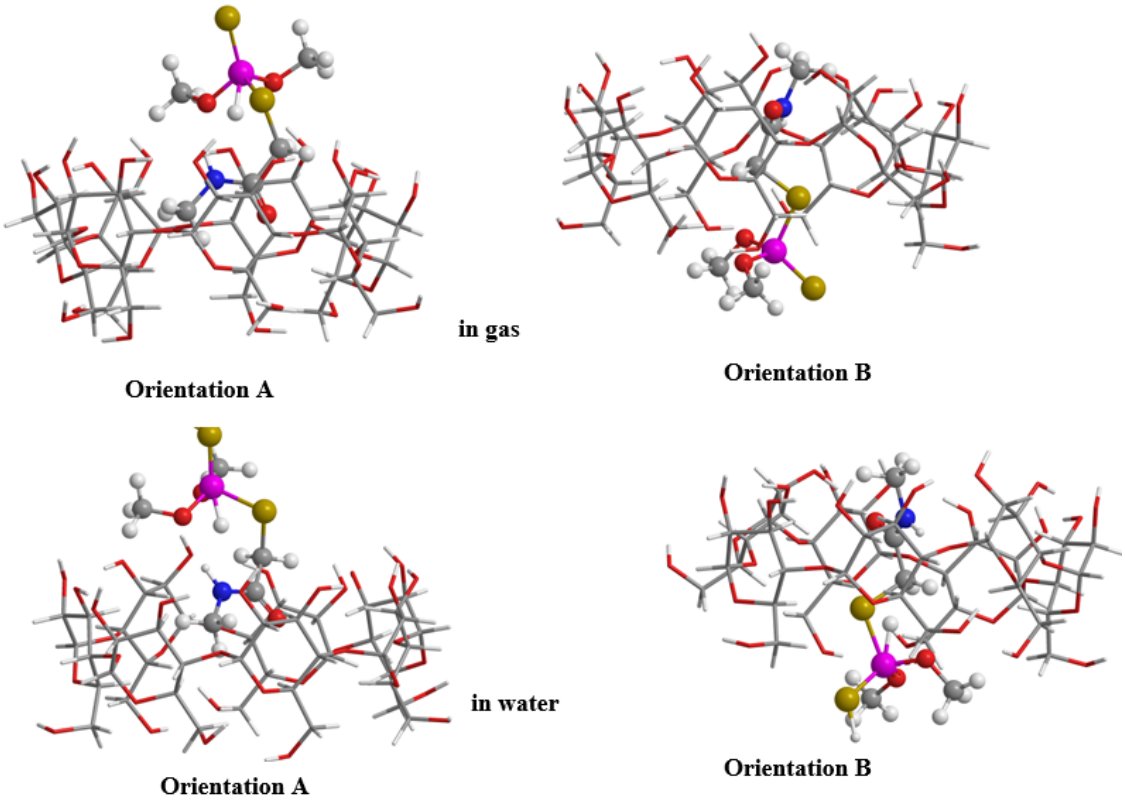

Figure 4

The optimized structures of the most stable conformations obtained at CAM- B3LYP/6–31 G (d, p) calculation in gas phase and in water

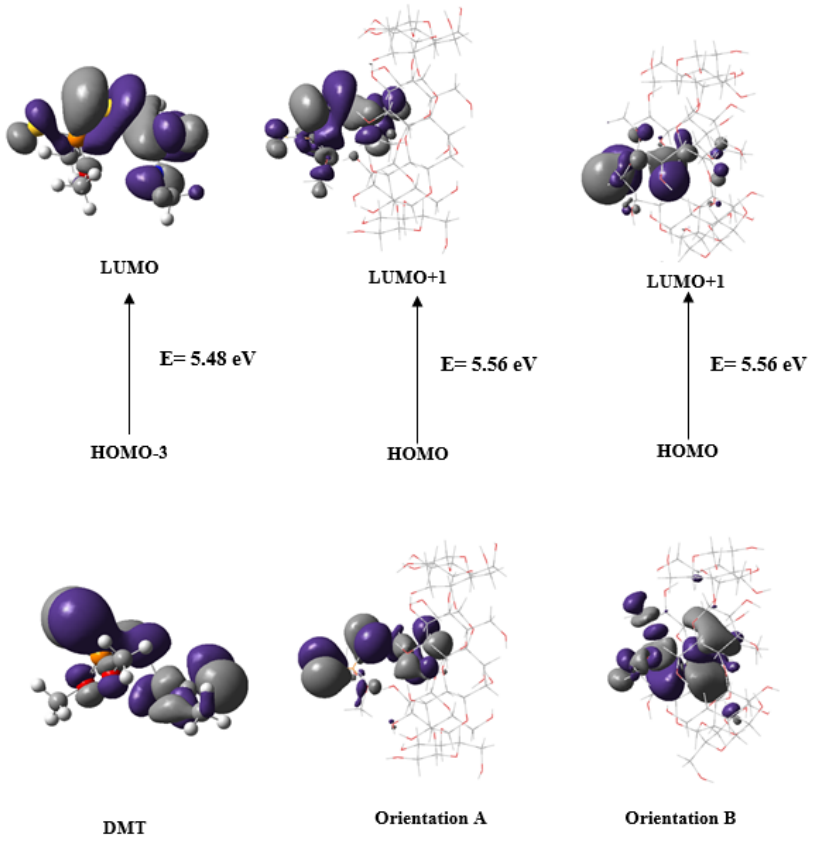

Figure 5

3D plots of the HOMO and LUMO orbital calculated from TD-DFT/ CAM-B3LYP/6–31 G (d, p) analysis in water

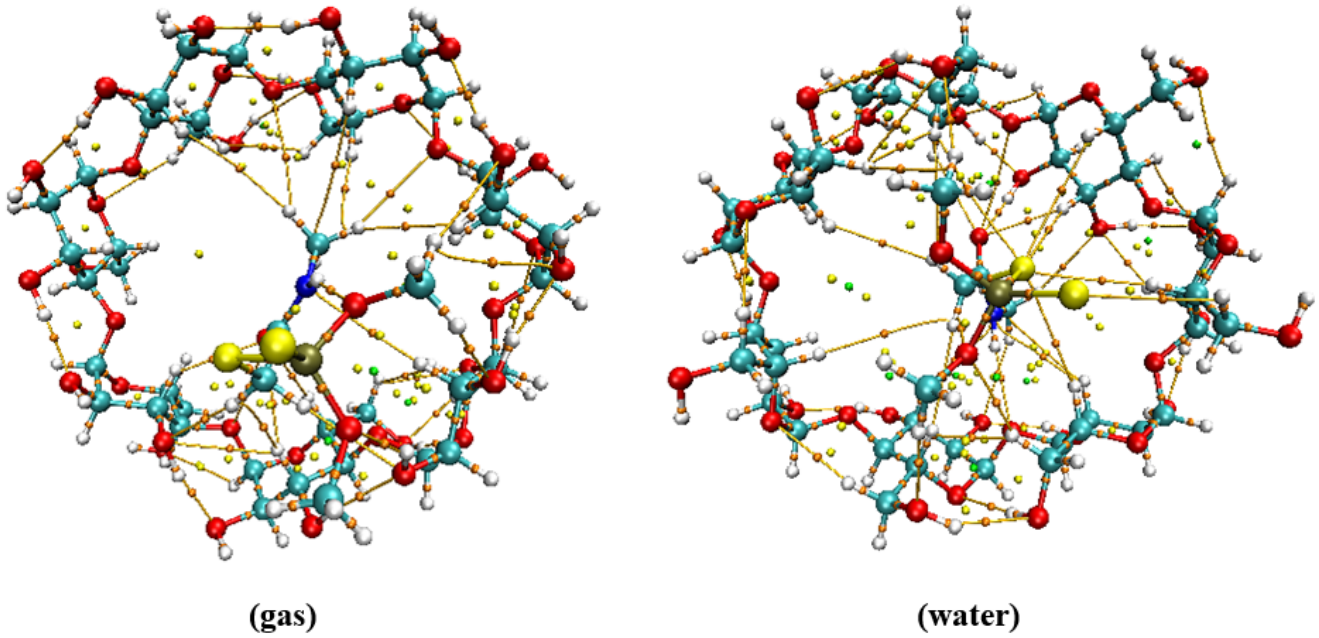

Figure 6

Molecular topography analysis of DMT@β-CD complex for orientation B in gas and water at CAM-B3LYP/6-31G (d, p) level.

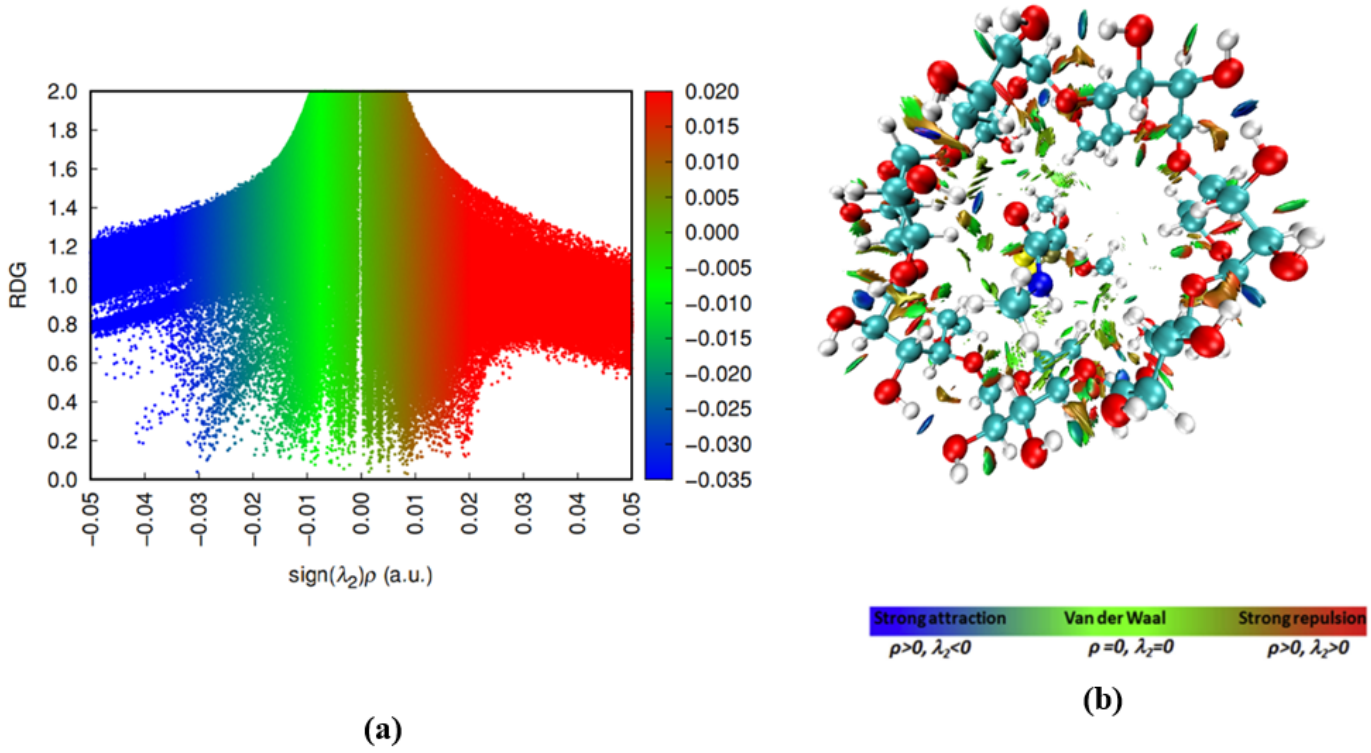

Figure 7

(a) Plots of reduced density gradient (s) versus the electron density multiplied by sign of second Hessian eigenvalue (sign λ_2) ρ, **(b)** visual weak interactions with NCI analysis of DMT@β-CD complex

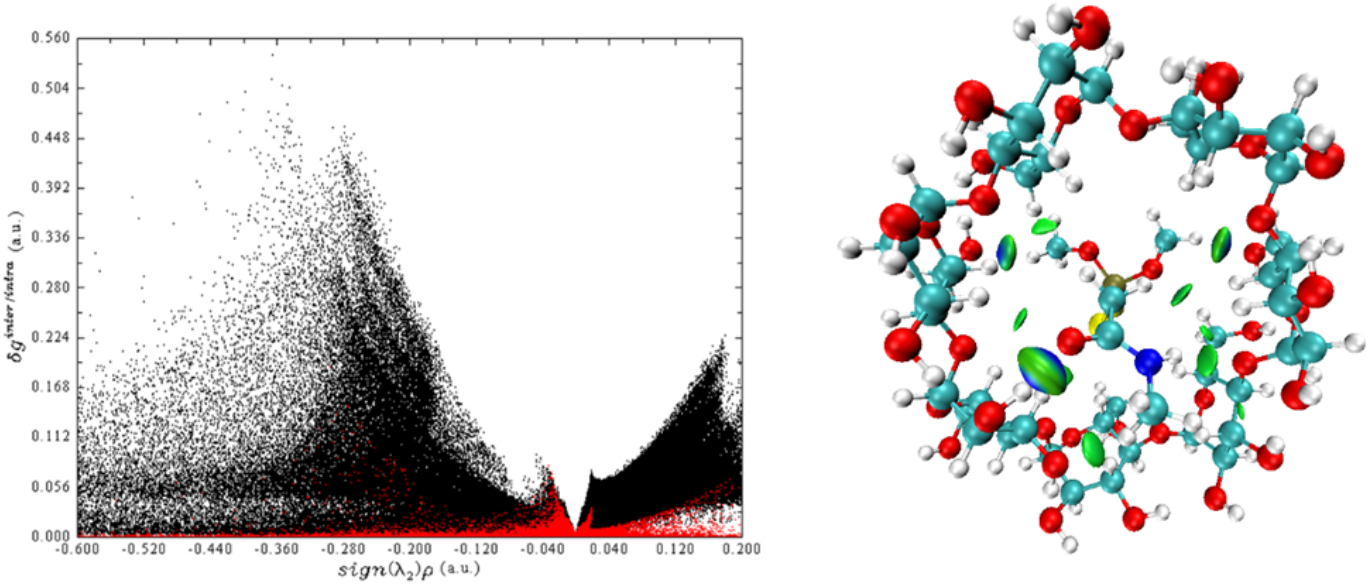

Figure 8

IGM isosurfaces and scatter plots of the DMT@β-CD complex

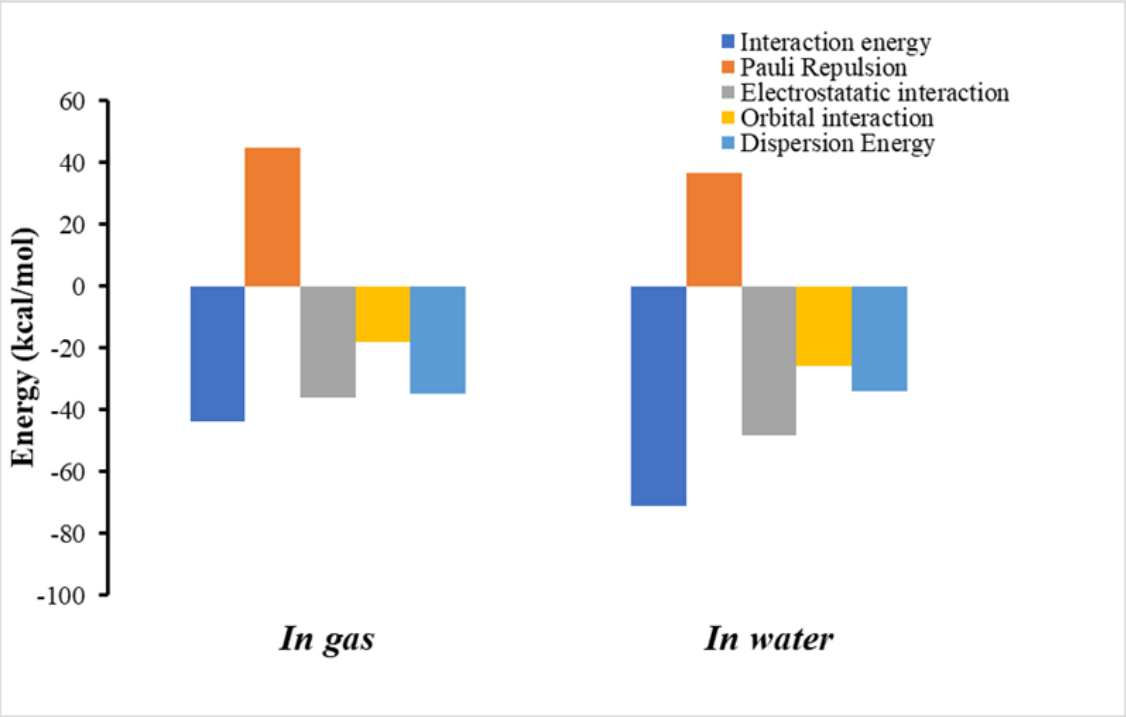

Figure 9

EDA component values for DMT@β-CD complex